

RatLesNetv2: A Fully Convolutional Network for Rodent Brain Lesion Segmentation

Juan Miguel Valverde, Artem Shatillo, Riccardo De Feo, Olli Grhn, Alejandra Sierra, and Jussi Tohka

Abstract—Segmentation of rodent brain lesions on magnetic resonance images (MRIs) is a time-consuming task with high inter- and intra-operator variability due to its subjective nature. We present a three-dimensional fully convolutional neural network (ConvNet) named RatLesNetv2 for segmenting rodent brain lesions. We compare its performance with other ConvNets on an unusually large and heterogeneous data set composed by 916 T2-weighted rat brain scans at nine different lesion stages. RatLesNetv2 obtained similar to higher Dice coefficients than the other ConvNets and it produced much more realistic and compact segmentations with notably less holes and lower Hausdorff distance. RatLesNetv2-derived segmentations also exceeded inter-rater agreement Dice coefficients. Additionally, we show that training on disparate ground truths leads to significantly different segmentations, and we study RatLesNetv2 generalization capability when optimizing for training sets of different sizes. RatLesNetv2 is publicly available at <https://github.com/jmlipman/RatLesNetv2>.

Index Terms—Lesion segmentation, Deep learning, Rat brain, Magnetic resonance imaging

I. INTRODUCTION

Rodents are widely used as models for drug discovery and the development of new treatments for human diseases. They account for more than 80% of the animals used in research in recent years [1]. In vivo imaging enables longitudinal studies on the same animal to investigate disease progression. However, magnetic resonance images (MRIs) can also include irrelevant areas for researchers. In order to facilitate subsequent work, a common practice is to segment meaningful regions by drawing their boundaries. In particular, the segmentation of lesions on rodent brain MRIs helps researchers to characterize the lesions by their size, the region where they are located, their shape, and their intensity values can also be subject to statistical analyses in MRI relaxometry.

The work of J.M. Valverde was funded from the European Union's Horizon 2020 Framework Programme (Marie Skłodowska Curie grant agreement #740264 (GENOMMED)) and R. De Feo's work was funded from Marie Skłodowska Curie grant agreement #691110 (MICROBRADAM). We also acknowledge the Academy of Finland grants (#275453 to A. Sierra and #316258 to J. Tohka). Part of the computational analysis was run on the servers provided by Bioinformatics Center, University of Eastern Finland, Finland.

J.M. Valverde, O. Grhn, A. Sierra and J. Tohka are with AI Virtanen Institute for Molecular Sciences, University of Eastern Finland, Kuopio 70150, Finland (e-mail: juanmiguel.valverde@uef.fi, olli.grohn@uef.fi, alejandra.sierralopez@uef.fi, jussi.tohka@uef.fi)

A. Shatillo is with Charles River Discovery Services, Kuopio 70210, Finland (e-mail: artem.shatillo@crl.com)

R. De Feo is with Centro Fermi - Museo Storico della Fisica e Centro Studi e Ricerche Enrico Fermi, Rome 00184, Italy, with Sapienza Università di Roma, 00185 Rome, Italy, and also with AI Virtanen Institute for Molecular Sciences, University of Eastern Finland, Kuopio 70150, Finland. (e-mail: riccardo.defeo@uniroma1.it)

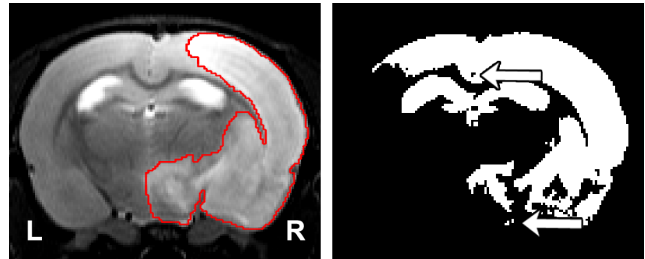


Fig. 1. Left: Representative lesion with its ground truth. Right: Segmentation of the lesion using thresholding where the threshold was found by maximizing the Dice coefficient with respect to the manual segmentation. The arrows indicate the presence of holes and islands (independently connected components) within and outside the mask respectively. The hippocampus was entirely misclassified as lesion.

Manual segmentation can be prohibitively time-consuming. Studies involving animals may acquire hundreds of three-dimensional (3D) images, and segmenting them manually may cause a bottleneck. In addition, the ill-posedness of the task leads to low inter- and intra-rater agreement. This discrepancy is especially severe in rodent brain lesion segmentation, in which the Dice coefficients [2] between two different human-made annotations can be as low as 0.73 [3] or 0.79 [4]. The quality of the segmentations depends on several factors such as the partial volume effect, the image contrast and the knowledge and experience of the annotators. Despite that, manual segmentation is the gold standard and a common practice among researchers who use animal models [5], [6].

Semi-automatic methods are a faster alternative to manual segmentation. However, they do not entirely overcome the subjectivity of the problem, as human interaction is required. Wang et al. [7] applied a combination of thresholds commonly used in the literature to segment lesions on apparent diffusion coefficient (ADC) maps and T2-weighted images. Afterwards, they performed various statistical analyses on 18 rats. Choi et al. [8] first normalized the intensity values of each image with respect to the left hemisphere of the brain, and they performed a series of thresholds to segment 1h permanent middle cerebral artery occlusion (MCAO) ischemic lesions in 31 diffusion-weighted images (DWI) of rat brain. These thresholding-based methods, as well as other voxel-wise approaches, disregard the spatial and contextual information of the images. Additionally, they are sensitive to the image modality, contrast and possible artifacts. Pipelines that include thresholding operations may lead to poor and inconsistent segmentation results in the form of holes within and outside the lesion mask (Fig. 1).

In recent years, few fully automated methods have been

proposed for lesion segmentation in rodents. Mulder et al. [4] developed a level-set based algorithm, and they tested it on 121 T2-weighted mouse brain scans. The data set included mice of different ages, scans at different time-points and annotations from two operators. However, the accuracy of their method relies on the performance of other independent steps such as registration, skull-stripping and contralateral ventricle segmentation. Arnaud et al. [9] derived a pipeline that detects anomalous voxels with respect to a reference model of healthy animals. This pipeline was tested on 53 rat brain MRI maps, such as ADC, T1 and T2, but it was specifically designed for quantitative MRIs, and the pipeline expects sham-operated animals in the data set, requirement that may not be always feasible.

Deep learning, and more specifically convolutional neural networks (ConvNets), has become increasingly popular due to its competitive performance on image-related tasks such as object classification [10], object detection [11] and image segmentation [12], including medical image segmentation [13]. Literature on medical image segmentation with ConvNets is dominated by approaches tested on human-derived data [14]–[18]. In contrast, rodent segmentation data sets are scarce and smaller in size [19], and consequently, it is difficult to find ConvNet architectures benchmarked on rodent images. A notable exception is [20], who developed a framework to extract brain tissue on human and mice MRI scans after traumatic brain injury.

We present RatLesNetv2, a 3D ConvNet for segmenting rodent brain lesions. We extend our earlier conference paper [3] by 1) improving our previous ConvNet, termed RatLesNet, with a deeper and different architecture; 2) providing an ablation study [21] of our network’s architecture; 3) testing RatLesNetv2 on a considerably larger and more heterogeneous data set composed by 916 MRI scans at 9 different lesion stages; 4) measuring the performance with additional metrics (compactness and Hausdorff distance); 5) studying the difference between predictions when the model is optimized for different ground truths; 6) assessing the model’s generalization capability on diverse training sets of different length and 7) making RatLesNetv2 publicly available.

We show that RatLesNetv2 generates more realistic segmentations than our previous RatLesNet and VoxResNet [22], a state-of-the-art ConvNet originally designed for volumetric human brain segmentation, when optimized for the same task. The accuracies of the masks derived with RatLesNetv2 also exceeded inter-rater agreement scores.

II. METHOD

We propose a 3D ConvNet named RatLesNetv2 for segmenting brain lesions on rodents. RatLesNetv2 is trained end-to-end, requiring no preprocessing such as skull-stripping or non-uniformity correction.

A. Convolutional neural networks

Convolutional neural networks (ConvNets) use stacks of convolutions to transform spatially correlated data, such as images, to extract their features. The first layers of the network

capture low-level information such as edges and corners, and the final layers extract more abstract features. The number of convolutions adjusts two attributes of ConvNets: the number of parameters and the depth of the network. An excessive number of parameters leads to overfitting—memorizing the training data—whereas an insufficient number of parameters constrains the model’s capability to learn. The depth of a model is associated with the number of times the input data is transformed and it also adjusts the area that influences the prediction—the receptive field (RF). Recent approaches reduce the model parameters while maintaining the same receptive field by using more stacked convolutions of smaller kernel size [23].

Model architectures based on U-Net [13] are very popular in medical image segmentation tasks. In contrast to patch-based models, the input images and the generated masks are the same size, which makes U-Nets computationally more efficient to train and to evaluate. The U-Net architecture resembles an auto-encoder with skip connections between the same levels of the encoder and decoder. The encoder transforms and reduces the dimensionality of the input images, and the decoder recovers the spatial information with the help of skip connections.

Skip connections also facilitate the gradient flow during back-propagation [24], but they are not sufficient to prevent the gradient of the loss to vanish, which makes the network harder to train. This is also referred as the vanishing gradient problem [25], and it particularly affects the final layers of the encoder part. Adding residual connections [25] along the network alleviates the vanishing gradient problem and it also yields in faster convergence rates during the training [24].

B. RatLesNetv2 architecture

RatLesNetv2 (Fig. 2) has three downsampling and three up-sampling stages connected via skip connections. Maxpooling downsamples the data with a window size and strides of 2, and trilinear interpolation upsamples the feature maps. Bottleneck layers (Fig. 2, green blocks) stack a ReLU activation function, a batch normalization (BatchNorm) layer [26] and a 3D convolution with kernel size of 1 that combines and modifies the number of channels of the feature maps from *in* to *out*. ResNetBlock layers (Fig. 2, orange blocks) contain two stacks of ReLU activations, BatchNorm, and 3D convolutions with kernel size of 3. Similarly to VoxResNet [22], the input and output of each block is summed in a ResNet-style [25]. The width of the blocks in the decoder is twice (64) with respect to the encoder part (32) due to the concatenation of previous layers in the same stage of the network.

At the end of the network, the probabilities $z_i, i = 1, 2$ are normalized by the Softmax function

$$\text{Softmax}(\mathbf{z})_i = \frac{e^{z_i}}{\sum_{j=1}^K e^{z_j}} \quad (1)$$

and the index of the channel (non-lesion vs. lesion) with the largest Softmax probability voxel-wise becomes the segmentation mask.

RatLesNetv2 architecture differs from our previous RatLesNet [3] in three aspects: 1) RatLesNetv2 has one

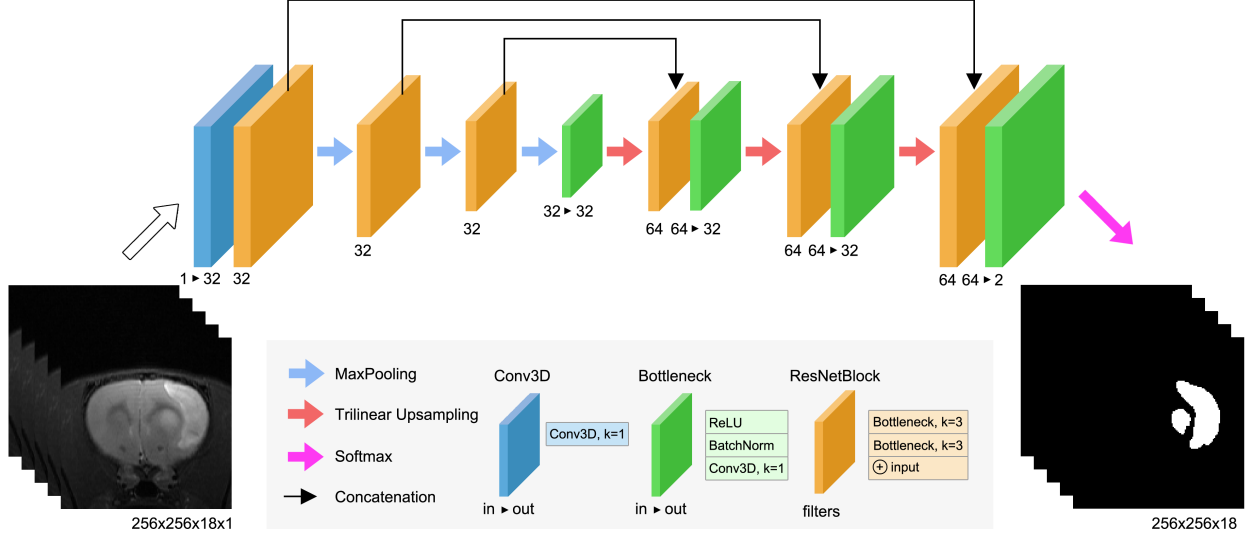


Fig. 2. RatLesNetv2 network architecture. See the text for the detailed explanation of the blocks.

more downsampling and upsampling levels, increasing the receptive field to $76 \times 76 \times 76$ voxels. This increment allows RatLesNetv2 to consider more information from a larger area. 2) RatLesNetv2 uses trilinear upsampling and 3) ResNet-Blocks to replace unpooling [27] and DenseNetBlocks [28], respectively, reducing memory usage and execution time.

C. Loss function

The parameters of ConvNets are optimized by minimizing a loss function that describes the difference between the predictions and the ground truth. RatLesNetv2 is optimized with Adam [29] by minimizing the combination of cross entropy and Dice loss functions $L_{total} = L_{BCE} + L_{Dice}$. Cross entropy is one of the most popular methods to describe the dissimilarity with respect to the ground truth; it measures the error as the difference between distributions. Since our annotations consist of only two classes (lesion and non-lesion) we used binary cross entropy

$$L_{BCE} = -\frac{1}{N} \sum_{i=1}^N p_i \cdot \log(q_i) + (1 - p_i) \cdot \log(1 - q_i) \quad (2)$$

where $p_i \in \{0, 1\}$ represents whether voxel i is lesion in the ground truth and $q_i \in [0, 1]$ is the predicted Softmax probability of lesion class. Dice loss [30] is defined as:

$$L_{Dice} = 1 - \frac{2 \sum_i^N p_i q_i}{\sum_i^N p_i^2 + \sum_i^N q_i^2} \quad (3)$$

The rationale behind using Dice loss is to directly maximize the Dice coefficient, one of the metrics to assess image segmentation performance. Although Dice loss' derivative can be unstable when its denominator is very small, the use of BatchNorm and skip connections helps during the optimization by smoothing the loss landscape [31], [32].

D. Post-processing

Since our model optimizes a per-voxel loss function, small undesirable clusters of voxels may appear disconnected from the main predicted mask. These spurious clusters may be referred as “islands” when they are separated from the largest connected component and “holes” when they are inside the lesion mask. Figure 1 illustrates these terms.

Small islands and holes can be removed in a final post-processing operation yielding in more realistic segmentations. The challenging follow-up question is: what is the maximum number of connected voxels to consider an island or hole small? A very small threshold will not eliminate enough small islands whereas a too large threshold may remove small lesions correctly identified. To answer this question, we calculated the distribution of the islands and holes' size and we chose a threshold such that 90% of the clusters were removed. Accordingly, post-processing operation disregards clusters of 20 voxels or less, within or outside the largest lesion mask.

E. Implementation

RatLesNetv2 was implemented in Pytorch [33] and it was run on a Ubuntu 16.04 with an Intel Xeon W-2125 CPU @ 4.00GHz processor, 64 GB of memory and an NVidia GeForce GTX 1080 Ti with 11 GB of memory. RatLesNetv2 is publicly available at <https://github.com/jmlipman/RatLesNetv2>

III. EXPERIMENTS AND RESULTS

A. Material

The data set consisted of 916 MR T2-weighted brain scans of different adult male Wistar rats weighting between 250-300 g. The data, provided by Discovery Services site of Charles River Laboratories¹, were derived from 12 different studies. Transient (120 min) focal cerebral ischemia was produced by

¹<https://www.criver.com/products-services/discovery-services>

TABLE I
NUMBER OF SCANS PER STUDY SEGREGATED BY LESION STAGE,
INCLUDING SHAM-OPERATED ANIMALS.

Study	2h	24h	D3	D7	D14	D21	D28	D35	Shams
A	12	12	0	0	0	0	0	0	24
B	0	46	0	0	0	0	0	0	3
C	0	59	0	0	0	0	0	0	1
D	0	162	0	0	0	0	0	0	4
E	0	0	0	0	0	0	0	20	1
F	0	33	30	0	30	0	27	0	46
G	0	0	0	53	0	0	0	0	12
H	0	45	0	0	0	0	0	0	0
I	0	0	64	0	0	0	62	0	0
J	0	32	0	0	0	0	0	0	0
K	0	17	0	0	0	0	0	0	0
L	0	0	41	0	0	40	0	0	40
Total	12	406	135	53	30	40	89	20	131

middle cerebral artery occlusion (tMCAO) in the right hemisphere of the brain [34]. MR data acquisitions were performed at different time-points after the occlusion (lesion stages, see Table I). Some studies also have sham-operated animals that underwent identical surgical procedures, but without the actual tMCAO occlusion. All animal experiments were conducted according to the National Institute of Health (NIH) guidelines for the care and use of laboratory animals, and approved by the National Animal Experiment Board, Finland. Multi-slice multi-echo sequence was used with the following parameters; TR = 2.5 s, 12 echo times (10-120 ms in 10 ms steps) and 4 averages in a horizontal 7T magnet. T2-weighted images were calculated as the sum of the all echoes. Eighteen coronal slices of 1 mm thickness were acquired using a field-of-view of 30x30 mm² and 256x256 imaging matrices of resolution 117 μ m \times 117 μ m.

The T2-weighted MR images and their corresponding lesion segmentation were provided in form of NIfTI files. We performed an additional independent manual segmentation of the lesions on the first study that we acquired (study A, Table I) to approximate inter-rater variability. The average Dice coefficient [2] between the two manual segmentations was 0.67 with a standard deviation of 0.12 on 2h lesions and 0.79 with a standard deviation of 0.08 on 24h lesions. The overall average was 0.73 ± 0.12 . Unless stated otherwise, we used our independent segmentation as the ground truth for study A.

We produced two different train/test set divisions. 1) In the first one, the training set contained the 48 scans of the study we segmented (study A) and the test set contained the remaining 868 images. The training set was further divided to training (36 images) and validation sets (12 images). This train/test division is referred to as “homogeneous” and its train/validation split has the same ratio 2h/24h time-points and sham/no-sham animals. 2) The second division had the same number of train/test images than “homogeneous”. The training set was divided into training (40 images) and validation (8 images) sets. This division is referred to as “heterogeneous” because the training set is more diverse as it contains scans

from every time-point and it maintains the same ratio in training and validation sets, i.e., 5 and 1 scan per time-point respectively.

B. Evaluation Metrics

In agreement with the literature [35], we argue that Dice coefficient alone is not an effective measure in rodent lesion segmentation and we complement it with two other metrics: a 3D compactness measurement and the Hausdorff distance.

1) *Dice coefficient* [2]: Dice coefficient is one of the most popular metrics in the field of image segmentation. It measures the overlap volume between two binary masks, typically the prediction of the model and the manually-annotated ground truth. Dice coefficient is formally described as:

$$Dice(A, B) = \frac{2|A \cap B|}{|A| + |B|} \quad (4)$$

where A and B are the segmentation masks.

2) *Compactness* [36]: Compact lesion masks are realistic and resemble human-made annotations. Compactness can be defined as the ratio between surface area (*area*) and volume of the mask (*volume*). More specifically, we define compactness as:

$$Compactness = area^{1.5}/volume \quad (5)$$

which has a constant minimum value of $6\sqrt{\pi}$ for any sphere. Consequently, low compactness values are desirable as they describe compact segmentations. Compactness measure penalizes holes and independently connected components because they increase the surface area with respect to its volume.

3) *Hausdorff distance* [37]: Hausdorff distance (HD) is defined as:

$$d(A, B) = \max \left\{ \max_{a \in \partial A} \min_{b \in \partial B} |a - b|, \max_{b \in \partial B} \min_{a \in \partial A} |a - b| \right\} \quad (6)$$

where A and B are the segmentation masks and ∂A and ∂B are their respective boundary voxels. It measures the maximum distance of the ground truth surface to the closest voxel of the prediction in millimeters, i.e, the largest segmentation error.

Hausdorff distance and compactness values were exclusively calculated in animals with lesions. Hausdorff distance values on slightly imperfect segmentations of sham-operated animals provide with excessively large values that distort the overall statistics. Additionally, compactness can not be calculated on empty volumes derived from scans without lesions. Since the anisotropy of the voxels affects these two metrics severely, we considered it when computing these measurements.

C. Training

RatLesNetv2, VoxResNet [22] and RatLesNet [3] were optimized in each task with Adam [29] ($\beta_1 = 0.9, \beta_2 = 0.999, \epsilon = 10^{-8}$), starting with a learning rate of 10^{-5} for 700 epochs. A small set of learning rates were tested on each architecture to ensure that we used the best performing learning rate in each model. Images were zero-centered and

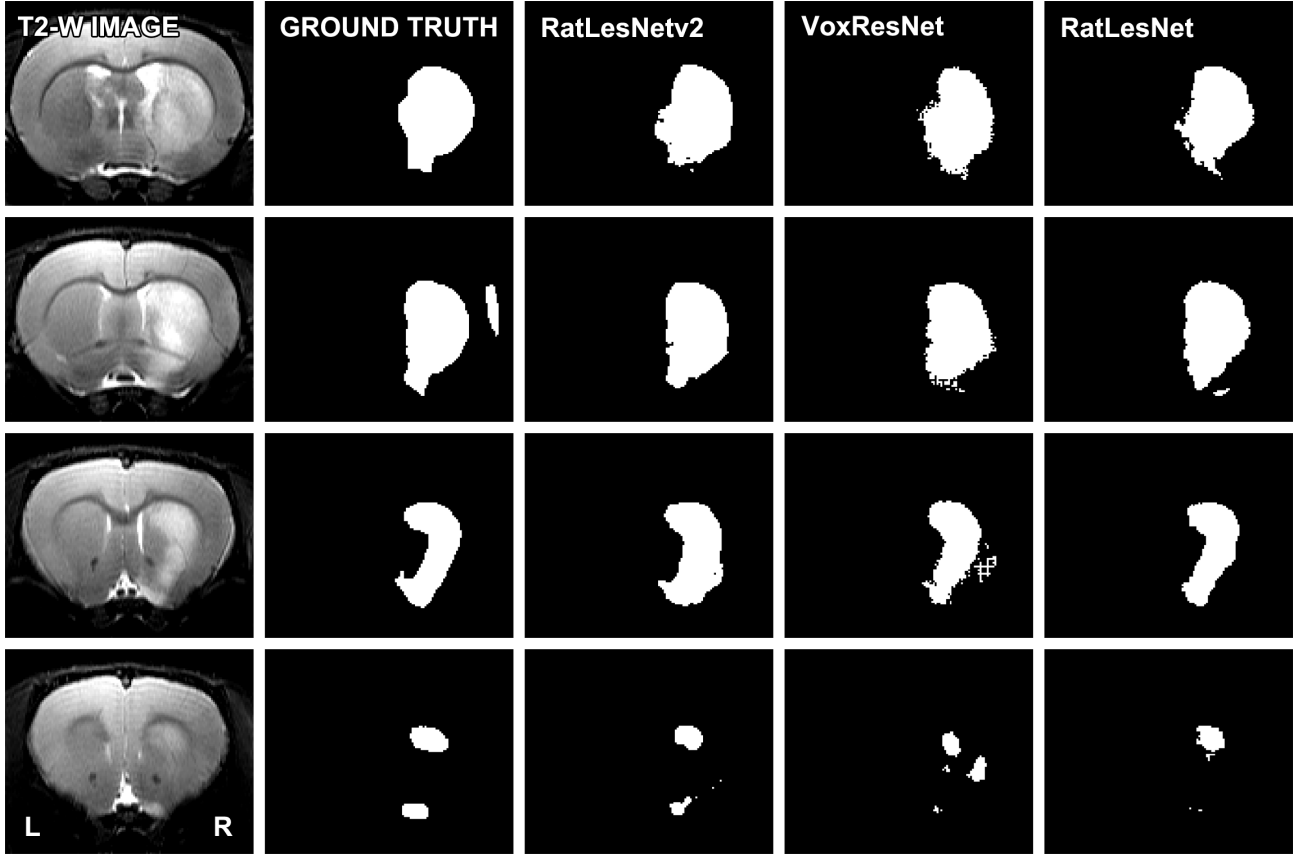


Fig. 3. Comparison of the segmentation masks of 4 consecutive slices. The depicted T2-weighted image corresponds to a typical scan, i.e., volume whose segmentation achieved the median Dice coefficient in the test set (heterogeneous division). Segmentations were not post-processed.

their variance was normalized to one. Models were trained three times and their performance was evaluated from the lesion masks derived with majority voting across the three independent runs. We confirmed that this strategy improves the performance (see Section III-D).

D. Performance of RatLesNetv2

We optimized RatLesNetv2, VoxResNet [22] and RatLesNet [3] on the homogeneous and heterogeneous data set divisions. 3D U-Net [38] was not evaluated due to the poor scores achieved in our earlier conference paper [3]. The results of the performance evaluation are in Table II. We assessed significance of performance difference through a paired permutation test with 10000 random iterations, and we highlight a significant difference with bold font in Table II. We used the usual 0.05 as the significance threshold. To understand the effects of post-processing, Table II includes results before and after applying post-processing. However, the hypothesis tests were only performed for the results after the post-processing. Figure 3 and the figures in Supplementary Material illustrate the quality of the segmentations produced by RatLesNetv2, VoxResNet and RatLesNet. The reported Dice coefficients, compactness values and Hausdorff distances are also included in Supplementary Material as CSV files.

Training networks three times with the same training set and deciding the voxel label by majority voting led to significantly better performance scores in all cases (all p -values < 0.006).

TABLE II
PERFORMANCE EVALUATION ON THE TEST SET BEFORE AND AFTER POST-PROCESSING. TOP: HOMOGENEOUS DIVISION. BOTTOM: HETEROGENEOUS DIVISION. BOLD: VALUES SIGNIFICANTLY BETTER THAN THE OTHER ARCHITECTURES (* $^1p = 0.012$, * $^2p = 0.013$, * $^3p = 0.011$).

Model	Dice	Compactness	HD
RatLesNetv2-post	0.801 \pm 0.20 ^{*1}	29.65 \pm 8.39 ^{*2}	3.35 \pm 4.14
RatLesNetv2	0.801 \pm 0.20	29.97 \pm 8.59	3.54 \pm 3.90
VoxResNet-post	0.785 \pm 0.20	35.94 \pm 12.26	3.24 \pm 3.38
VoxResNet	0.785 \pm 0.20	36.81 \pm 12.79	3.65 \pm 2.98
RatLesNet-post	0.786 \pm 0.19	34.57 \pm 11.06	3.56 \pm 3.38
RatLesNet	0.785 \pm 0.19	35.21 \pm 11.39	4.16 \pm 2.70
RatLesNetv2-post	0.837 \pm 0.16	23.85 \pm 5.08 ^{*3}	3.59 \pm 3.60
RatLesNetv2	0.836 \pm 0.16	23.96 \pm 5.21	3.74 \pm 3.50
VoxResNet-post	0.837 \pm 0.16	29.45 \pm 6.82	3.15 \pm 3.07
VoxResNet	0.837 \pm 0.16	29.99 \pm 7.21	3.62 \pm 3.27
RatLesNet-post	0.838 \pm 0.15	27.66 \pm 6.11	3.69 \pm 3.03
RatLesNet	0.838 \pm 0.15	27.97 \pm 6.18	3.99 \pm 3.17

This strategy increased Dice coefficients by an average of 3% and decreased compactness and Hausdorff distances by an average of 7% and 21% with respect to the first run.

Dice coefficients had a large standard deviation regardless of the architecture (from 0.15 to 0.20). However, note that the sample-wise difference between the Dice coefficients of RatLesNetv2 and VoxResNet had a smaller standard deviation

TABLE III
PERFORMANCE EVALUATION ON THE TEST SET AFTER POST-PROCESSING
SEGREGATED BY LESION STAGE. TOP: HOMOGENEOUS DIVISION.
BOTTOM: HETEROGENEOUS DIVISION.

Time-point (scans)	Dice	Compactness	HD
24h (394)	0.827 \pm 0.17	26.77 \pm 5.30	3.30 \pm 3.50
D3 (135)	0.762 \pm 0.14	31.21 \pm 8.54	2.95 \pm 2.79
D7 (53)	0.768 \pm 0.13	43.53 \pm 10.99	2.96 \pm 4.43
D14 (30)	0.713 \pm 0.21	36.65 \pm 10.30	3.89 \pm 6.83
D21 (40)	0.789 \pm 0.11	32.94 \pm 6.65	2.65 \pm 1.03
D28 (89)	0.575 \pm 0.30	28.54 \pm 7.26	4.55 \pm 6.58
D35 (20)	0.734 \pm 0.26	27.34 \pm 6.59	3.48 \pm 5.77
shams (107)	1.000 \pm 0.00	—	—
2h (6)	0.745 \pm 0.05	28.06 \pm 4.89	3.63 \pm 2.55
24h (400)	0.824 \pm 0.14	24.08 \pm 5.13	4.22 \pm 3.85
D3 (129)	0.807 \pm 0.11	24.34 \pm 6.19	2.86 \pm 2.55
D7 (47)	0.855 \pm 0.11	24.04 \pm 3.13	2.48 \pm 3.42
D14 (24)	0.836 \pm 0.14	22.10 \pm 4.24	1.75 \pm 0.94
D21 (34)	0.860 \pm 0.10	23.58 \pm 2.32	2.97 \pm 3.52
D28 (83)	0.685 \pm 0.25	22.49 \pm 4.61	3.07 \pm 2.82
D35 (14)	0.769 \pm 0.27	22.34 \pm 3.15	3.72 \pm 6.91
shams (131)	1.000 \pm 0.00	—	—

of 0.07, i.e., the Dice values were correlated. Large standard deviations have been previously reported in literature [3], [4] and they are present even in the inter-rater disagreement of human-made annotations that rely on a semi-automatic segmentation pipeline [4]. This high variability may arise due to the ill-posedness and subjectivity of the segmentation task, and it shows that reporting Dice coefficients alone might not be sufficient for this type of segmentation problems. As an example, given a brain with a very large and a very small lesion, if the segmentation accurately predicts the large lesion and ignores the small one, unlike Hausdorff distance, Dice coefficients will not effectively reflect the error in the small lesion. Likewise, a lesion segmentation with a crispy surface and several small holes and islands may have a high Dice coefficient despite being unrealistic.

RatLesNetv2 yielded more compact segmentations than its competitors. Table II shows that RatLesNetv2 achieved significantly better compactness values (all p-values < 0.013) than VoxResNet and RatLesNet. Remarkably, VoxResNet produced masks with several more holes and islands, leading to less compact segmentations. Figure 3 (VoxResNet column) illustrates this problem. The average compactness values of RatLesNetv2 were higher than the ground truth (20.98 ± 3.28 , $p = 0.002$). However, this was expected as human annotators are likely to produce segmentations with excessively rounded boundaries. VoxResNet predictions after post-processing obtained the lowest Hausdorff distance, but VoxResNet’s Hausdorff distance values were not significantly different from RatLesNet’s or RatLesNetv2’s.

Post-processing had little to no effect on the average Dice coefficients, but it enhanced the final segmentation quality as it removed spurious clusters of voxels. This improvement is reflected in the reduction of compactness values and the considerable decrease of Hausdorff distances. Remarkably,

TABLE IV
ABLATION STUDY. TOP: HOMOGENEOUS TASK. BOTTOM:
HETEROGENEOUS TASK. *: SAME NUMBER OF PARAMETERS THAN
BASELINE. BOLD: BASELINE SIGNIFICANTLY BETTER. ITALIC: BASELINE
SIGNIFICANTLY WORSE (P-VALUES < 0.05).

Study	Dice	Compactness	HD
Baseline	0.801 \pm 0.20	29.97 \pm 8.59	3.54 \pm 3.90
DenseNetBlock*	0.797 \pm 0.20	29.62 \pm 8.19	4.05 \pm 3.68
Halving RF	0.799 \pm 0.20	30.18 \pm 9.15	3.96 \pm 3.68
Halving RF*	0.798 \pm 0.20	31.45 \pm 10.29	4.45 \pm 3.49
Width-28	0.800 \pm 0.20	32.39 \pm 9.66	4.25 \pm 3.86
Width-36	0.798 \pm 0.20	30.81 \pm 9.35	3.30 \pm 2.89
Baseline	0.836 \pm 0.16	23.96 \pm 5.21	3.74 \pm 3.50
DenseNetBlock*	0.837 \pm 0.16	23.68 \pm 4.65	3.96 \pm 3.33
Halving RF	0.838 \pm 0.16	24.78 \pm 5.25	3.56 \pm 3.02
Halving RF*	0.846 \pm 0.15	24.99 \pm 5.12	3.88 \pm 3.40
Width-28	0.843 \pm 0.16	23.02 \pm 4.31	3.19 \pm 2.74
Width-36	0.843 \pm 0.16	23.83 \pm 4.70	3.65 \pm 3.04

the difference between before and after post-processing in the Hausdorff distance was more pronounced in VoxResNet and RatLesNet. In other words, RatLesNetv2 produced fewer segmentation errors far from the lesion surface.

To understand the performance of RatLesNetv2 in detail, results were segregated by lesion stage in Table III. Interestingly, there was no significant difference ($p = 0.125$) between the Dice coefficients of 24h scans derived from optimizing for homogeneous and heterogeneous training sets, despite heterogeneous training set having almost half 24h lesion brains (5 scans vs. 9 scans). However, Hausdorff distances were significantly higher ($p < 0.012$) on the 24h predictions generated by the model trained on the homogeneous division. This demonstrates that Dice coefficient alone could not measure the significant improvement of training on more samples, and therefore it is crucial to consider complementary metrics to evaluate automatic segmentations.

Remarkably, despite training solely on 2h, 24h and sham-operated animals (homogeneous division, top of Table III) RatLesNetv2 extrapolated relatively well on every other time-point. Although the size, location and voxel intensity of the lesions were not the same across time-points, different lesions shared some characteristics that aided the network to generalize on unseen time-points. Dice coefficients, compactness values and Hausdorff distances deteriorated as the time-point was farther from 2h and 24h.

Training on the heterogeneous training set improved the Dice coefficients and compactness values of every model (Table II) and every time-point (Table III) with respect to homogeneous division, except on 24h lesions. Furthermore, it decreased variability. This indicates that RatLesNetv2 is capable of learning from a heterogeneous data set, and increasing diversity improves its performance.

RatLesNetv2 recognized animals without lesions notably well even if they were not part of the training set (heterogeneous division) providing average Dice coefficients of 1.0 on sham-operated animals even without post-processing. Additionally, Dice coefficients on 2h lesions, 24h lesions and

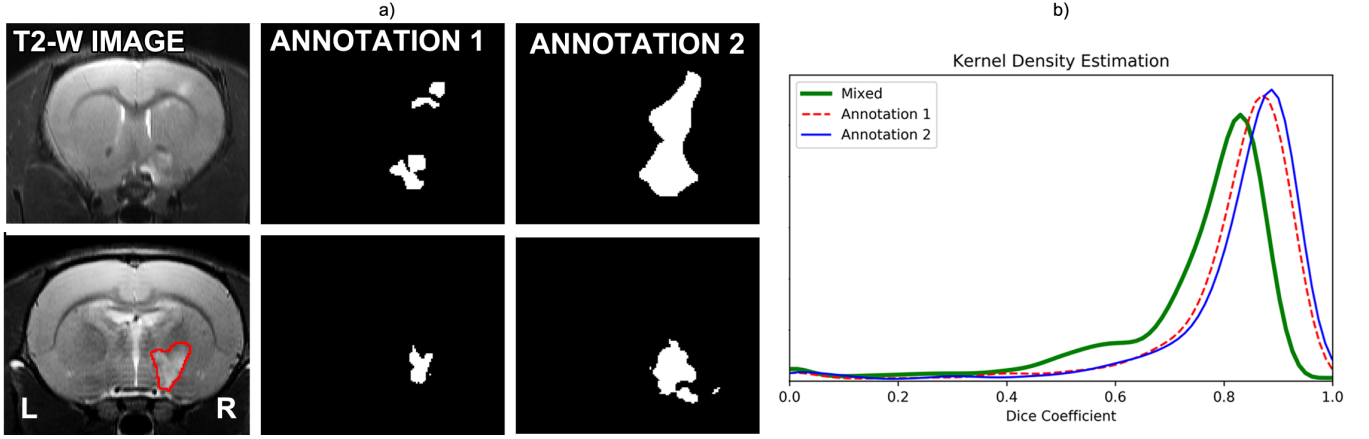


Fig. 4. a) (top row): Scan with the most disparate annotations between operator 1 and 2. a) (bottom row): Random scan with its ground truth and predictions when optimized for annotation 1 and 2 respectively. b): Kernel density estimation of three sets of Dice coefficients. Red (dashed line) and blue (solid line) estimations were calculated between the predictions of the model optimized for the same ground truth. Green (thick solid line) estimation was computed between the predictions whose model was optimized for different ground truths. The predictions generated when the same model is optimized for different ground truths are notably different.

overall were higher than inter-rater agreement.

E. Ablation studies

In order to comprehend the effects of the characteristics of RatLesNetv2 architecture, we conducted an ablation study [21] in which we changed or removed some parts of the model (Table IV).

1) *DenseNetBlock*: Similarly to RatLesNet [3], DenseNet-style [28] blocks were implemented in RatLesNetv2 while keeping the same number of parameters of the baseline RatLesNetv2 model. Although Dice coefficients and compactness values were similar, Hausdorff distances were significantly deteriorated with respect to RatLesNetv2 (all p -values < 0.019). The standard deviation of the sample-wise difference between the compactness values of DenseNetBlock and Baseline in the homogeneous division was 2.725, which explains why the difference was significant albeit it was small. Additionally, the use of DenseNetBlocks demanded notably more memory due to the concatenation operation. Therefore, DenseNetBlocks are not used by RatLesNetv2.

2) *Halving the receptive field (RF)*: The third downsampling stage of RatLesNetv2 was eliminated in order to reduce the receptive field from 72 voxels to 36. An additional test (marked in Table IV with an *) matched the number of parameters to the baseline. The reduction of the receptive field yielded in tiny improvements of the Dice coefficient in the heterogeneous division that were not significantly different from the baseline ($p = 0.068$). On the other hand, compactness values were slightly higher and Hausdorff distances were significantly larger than the baseline ($p < 0.033$), except in the heterogeneous division with less parameters. These results indicate that although a large receptive field does not bring considerable improvements measurable by the voxel-wise Dice coefficient, it helps reducing the largest segmentation error. This improvement of the Hausdorff distances may occur because the ConvNet is aware of a larger context.

3) *Width*: We increased and decreased the number of filters of RatLesNetv2 by 4 (Table IV, Width-28 and Width-36). This modification presented contradictory results between homogeneous and heterogeneous divisions across the three metrics. Dice coefficients, compactness values and Hausdorff distances were generally better than the baseline in the heterogeneous division and worse in the homogeneous division.

F. On the influence of disparate ground truths

The outcome of supervised learning algorithms is conditioned by the annotator's experience because his or her personal interpretation of the data affects the ground truth, which influences the algorithm's performance. In this experiment, we studied the effect of training RatLesNetv2 on different segmentations annotated by two operators, which can be seen as an inter-rater variability study of the same ConvNet with disparate knowledge.

We run RatLesNetv2 three times for each ground truth on the homogeneous training data, which come exclusively from the study with the two annotations (Study A, Table I). RatLesNetv2 produced 6 sets of 868 masks $\hat{y}_{g,r}$ where $g \in \{1, 2\}$ refers to the annotator segmenting the training data and $r \in \{1, 2, 3\}$ refers to the run. First, we approximated the intra-rater variability of RatLesNetv2 by calculating the Dice coefficients among the three runs for each ground truth separately, i.e., $\{dice(\hat{y}_{g,1}, \hat{y}_{g,2}), dice(\hat{y}_{g,2}, \hat{y}_{g,3}), dice(\hat{y}_{g,1}, \hat{y}_{g,3})\}$ for $g = 1, 2$. This led to two sets of 3 Dice coefficients per mask. Second, we calculated the Dice coefficient of the masks across the different ground truths $\{dice(\hat{y}_{1,i}, \hat{y}_{2,j})\}$ for $i, j = 1, 2, 3$ to approximate inter-rater similarity, leading to 9 Dice coefficients per mask.

The Dice coefficients of the predictions generated when optimizing for the same ground truth follow a distribution with a similar shape (Fig. 4 b), Annotation 1 and 2). In other words, the three sets of predictions $\hat{y}_{1,1}, \hat{y}_{1,2}, \hat{y}_{1,3}$ were similar among themselves in the same manner as $\hat{y}_{2,1}, \hat{y}_{2,2}, \hat{y}_{2,3}$. In contrast, the shape of the distribution of the Dice coefficients

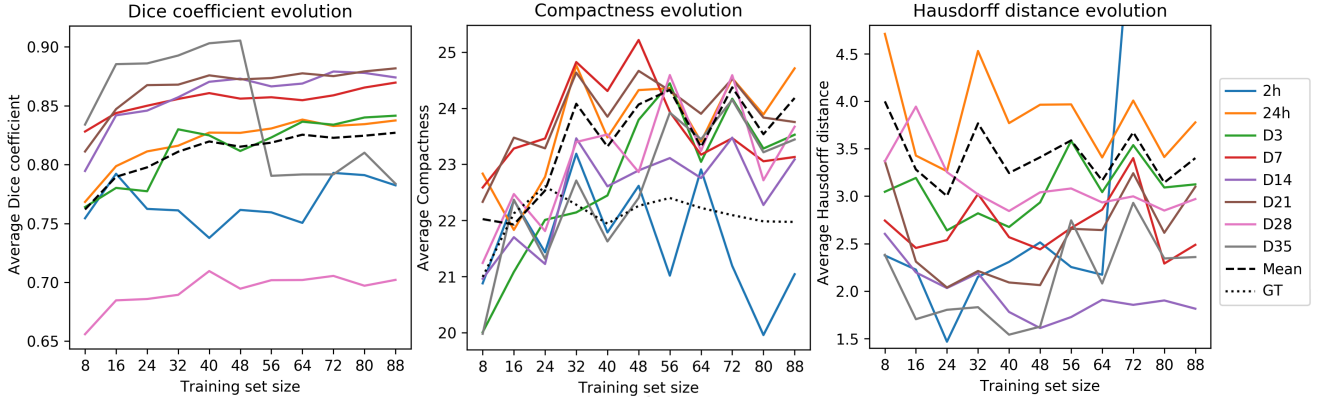


Fig. 5. RatLesNetv2 performance when optimizing for training sets of multiple sizes. Metrics (from left to right: Dice coefficient, compactness and Hausdorff distance) were processed from the masks derived with the majority voting across three runs on a fixed test set (828 images). Averages were segregated by time-point. Compactness graph includes the average compactness of the ground truth (dotted line).

that compare masks derived from different annotations (Fig. 4 b), Mixed) is notably different. Annotation 1 and Mixed values, and Annotation 2 and Mixed values were significantly different (p -values < 0.002). These results indicate that the predictions generated when the same model is optimized for disparate ground truths are different. Consequently, the quality of the manually-annotated ground truth has a direct impact on the quality of the lesion masks generated automatically.

After a visual inspection, we observed that Annotation 2 is more approximate, with simpler contours, than Annotation 1. Figure 4 a) (top row) shows the manual segmentations of the scan with the most disparate annotations and Fig. 4 a) (bottom row) shows the predictions on a scan with the highest Dice coefficient on our baseline study when RatLesNetv2 was trained on the different annotations. Thus, we hypothesize that the shift in the Annotation 2 distribution reflecting slightly higher Dice coefficients than Annotation 1 is due to the use of annotations that are easier to learn.

G. The impact of the training set size on the performance

Results in Section III-D corroborate that training on a diverse data set increases the model’s capability to extrapolate. As extrapolability is also affected by the size of the training set, it is essential to understand the relation between training set size and generalization capability.

In this experiment, we optimized RatLesNetv2 with training sets of different sizes. The training sets had the same ratio of time-points, i.e., we enlarged the training sets by 1 sample per time-point. Since the lowest number of samples across time-points corresponds to 12 (2h lesions) and we want to keep at least 1 image per time-point in the test set, we produced 11 training sets T_i of size $|T_i| = 8i$ for $i = 1, \dots, 11$, where 8 is the number of lesion stages.

Figure 5 illustrates the evolution of the Dice coefficients, compactness values and Hausdorff distances as the training set increases in size. Dice coefficients (Fig. 5, left) were remarkably different across time-points and almost every time-point reached a performance plateau with large data sets. Time-points 24h and D3—which composed the majority of the

test set scans by 56.7% and 17.8% of the total respectively—reached their plateaus later. This effect can be a consequence of the variability within samples. On the contrary, the time-points with the lowest number of samples (2h and D35 lesions with 1 and 9 image respectively) exhibited fluctuations.

Compactness values (Fig. 5, center) oscillated considerably regardless of the time-point. Contrary to one’s first intuition, compactness values increased analogously to the training set size. In other words, enlarging the training set yielded in less compact segmentations. Average compactness values on the test set (dashed line) follow a similar trend to average compactness values on the training set (dotted line). So, we hypothesize that the increase in compactness is due to optimizing for a wider variety of shapes. Yet, these compactness values were markedly lower than the compactness values derived from segmentations produced by VoxResNet and RatLesNet (Section III-D).

Hausdorff distances (Fig. 5, right) wobbled unstably along every time-point. Time-points with the largest number of samples (24h and D3) yielded in larger Hausdorff distances, likely due to the existence of outliers.

IV. CONCLUSION

We presented and made publicly available RatLesNetv2, a 3D ConvNet to segment rodent brain lesions. RatLesNetv2 has been evaluated on an exceptionally large and diverse data set of 916 rat brain MRIs and it exceeded overall inter-rater agreement Dice coefficients (inter-rater: 0.73 ± 0.12 , RatLesNetv2: 0.84 ± 0.16).

As Dice coefficient provides a limited overview of segmentation quality, we complemented it with two additional metrics: compactness and Hausdorff distance. RatLesNetv2 achieved overall better performance than our previous work and another state-of-the-art 3D ConvNet designed for medical image segmentation (VoxResNet [22]). This translates into segmentations with fewer spurious voxels over the mask, smoother surface and lower Hausdorff distance. In other words, RatLesNetv2 produced more realistic segmentations that resemble more to the ground truth.

We demonstrated that there is a significant difference between segmentations generated when RatLesNetv2 was optimized for different ground truths. Consequently, the quality of the ground truth affects the generated segmentations. As there is no unique definition of “lesion”, it may be advantageous for an algorithm to perform differently depending exclusively on the labels of the training set. On the other hand, it may also be desirable to design a robust algorithm that performs consistently regardless of some changes in the annotations.

Based on our experiments and, more specifically, the accuracy greater than inter-rater agreement and than of other ConvNets, RatLesNetv2 can be used to automate lesion segmentation in preclinical MRI studies on rats.

REFERENCES

- [1] S. Dutta and P. Sengupta, “Men and mice: relating their ages,” *Life sciences*, vol. 152, pp. 244–248, 2016.
- [2] L. R. Dice, “Measures of the amount of ecologic association between species,” *Ecology*, vol. 26, no. 3, pp. 297–302, 1945.
- [3] J. M. Valverde, A. Shatillo, R. De Feo, O. Gröhn, A. Sierra, and J. Tohka, “Automatic rodent brain mri lesion segmentation with fully convolutional networks,” in *International Workshop on Machine Learning in Medical Imaging*. Springer, 2019, pp. 195–202.
- [4] I. A. Mulder, A. Khmelinskii, O. Dzyubachyk, S. de Jong, N. Rieff, M. J. Wermer *et al.*, “Automated ischemic lesion segmentation in mri mouse brain data after transient middle cerebral artery occlusion,” *Frontiers in neuroinformatics*, vol. 11, p. 3, 2017.
- [5] R. De Feo and F. Giovè, “Towards an efficient segmentation of small rodents brain: a short critical review,” *Journal of neuroscience methods*, vol. 323, pp. 82–89, 2019.
- [6] A. Moraga, V. Gómez-Vallejo, M. I. Cuartero, B. Szczupak, E. San Sebastián, I. Markuerkiaga *et al.*, “Imaging the role of toll-like receptor 4 on cell proliferation and inflammation after cerebral ischemia by positron emission tomography,” *Journal of Cerebral Blood Flow & Metabolism*, vol. 36, no. 4, pp. 702–708, 2016.
- [7] Y. Wang, P.-T. Cheung, G. X. Shen, I. Bhatia, E. X. Wu, D. Qiu *et al.*, “Comparing diffusion-weighted and t2-weighted mr imaging for the quantification of infarct size in a neonatal rat hypoxic-ischemic model at 24 h post-injury,” *International journal of developmental neuroscience*, vol. 25, no. 1, pp. 1–5, 2007.
- [8] C.-H. Choi, K. S. Yi, S.-R. Lee, Y. Lee, C.-Y. Jeon, J. Hwang *et al.*, “A novel voxel-wise lesion segmentation technique on 3.0-t diffusion mri of hyperacute focal cerebral ischemia at 1 h after permanent mcao in rats,” *Journal of Cerebral Blood Flow & Metabolism*, vol. 38, no. 8, pp. 1371–1383, 2018.
- [9] A. Arnaud, F. Forbes, N. Coquery, N. Collomb, B. Lemasson, and E. L. Barbier, “Fully automatic lesion localization and characterization: Application to brain tumors using multiparametric quantitative mri data,” *IEEE transactions on medical imaging*, vol. 37, no. 7, pp. 1678–1689, 2018.
- [10] M. Tan and Q. V. Le, “Efficientnet: Rethinking model scaling for convolutional neural networks,” *arXiv preprint arXiv:1905.11946*, 2019.
- [11] S. Ren, K. He, R. Girshick, and J. Sun, “Faster r-cnn: Towards real-time object detection with region proposal networks,” in *Advances in neural information processing systems*, 2015, pp. 91–99.
- [12] L.-C. Chen, G. Papandreou, F. Schroff, and H. Adam, “Rethinking atrous convolution for semantic image segmentation,” *arXiv preprint arXiv:1706.05587*, 2017.
- [13] O. Ronneberger, P. Fischer, and T. Brox, “U-net: Convolutional networks for biomedical image segmentation,” in *International Conference on Medical image computing and computer-assisted intervention*. Springer, 2015, pp. 234–241.
- [14] B. H. Menze, A. Jakab, S. Bauer, J. Kalpathy-Cramer, K. Farahani, J. Kirby *et al.*, “The multimodal brain tumor image segmentation benchmark (brats),” *IEEE transactions on medical imaging*, vol. 34, no. 10, pp. 1993–2024, 2014.
- [15] P. Bilic, P. F. Christ, E. Vorontsov, G. Chlebus, H. Chen, Q. Dou *et al.*, “The liver tumor segmentation benchmark (lits),” *arXiv preprint arXiv:1901.04056*, 2019.
- [16] M. Dolejsi, J. Kybic, M. Polovincak, and S. Tuma, “The lung time: Annotated lung nodule dataset and nodule detection framework,” in *Medical Imaging 2009: Computer-Aided Diagnosis*, vol. 7260. International Society for Optics and Photonics, 2009, p. 72601U.
- [17] O. Maier, B. H. Menze, J. von der Gabelntz, L. Häni, M. P. Heinrich, M. Liebrand *et al.*, “Isles 2015-a public evaluation benchmark for ischemic stroke lesion segmentation from multispectral mri,” *Medical image analysis*, vol. 35, pp. 250–269, 2017.
- [18] N. Heller, N. Sathianathan, A. Kalapara, E. Walczak, K. Moore, H. Kaluzniak *et al.*, “The kits19 challenge data: 300 kidney tumor cases with clinical context, ct semantic segmentations, and surgical outcomes,” *arXiv preprint arXiv:1904.00445*, 2019.
- [19] I. A. Mulder, A. Khmelinskii, O. Dzyubachyk, S. De Jong, M. J. Wermer, M. Hoehn *et al.*, “Mri mouse brain data of ischemic lesion after transient middle cerebral artery occlusion,” *Frontiers in neuroinformatics*, vol. 11, p. 51, 2017.
- [20] S. Roy, A. Knutsen, A. Korotcov, A. Bosomtvi, B. Dardzinski, J. A. Butman *et al.*, “A deep learning framework for brain extraction in humans and animals with traumatic brain injury,” in *2018 IEEE 15th International Symposium on Biomedical Imaging (ISBI 2018)*. IEEE, 2018, pp. 687–691.
- [21] R. Meyes, M. Lu, C. W. de Puiseau, and T. Meisen, “Ablation studies in artificial neural networks,” *ArXiv*, vol. abs/1901.08644, 2019.
- [22] H. Chen, Q. Dou, L. Yu, J. Qin, and P.-A. Heng, “Voxresnet: Deep voxelwise residual networks for brain segmentation from 3d mr images,” *NeuroImage*, vol. 170, pp. 446–455, 2018.
- [23] C. Szegedy, V. Vanhoucke, S. Ioffe, J. Shlens, and Z. Wojna, “Rethinking the inception architecture for computer vision,” in *Proceedings of the IEEE conference on computer vision and pattern recognition*, 2016, pp. 2818–2826.
- [24] M. Drozdal, E. Vorontsov, G. Chartrand, S. Kadoury, and C. Pal, “The importance of skip connections in biomedical image segmentation,” in *Deep Learning and Data Labeling for Medical Applications*. Springer, 2016, pp. 179–187.
- [25] K. He, X. Zhang, S. Ren, and J. Sun, “Deep residual learning for image recognition,” in *Proceedings of the IEEE conference on computer vision and pattern recognition*, 2016, pp. 770–778.
- [26] S. Ioffe and C. Szegedy, “Batch normalization: Accelerating deep network training by reducing internal covariate shift,” *arXiv preprint arXiv:1502.03167*, 2015.
- [27] H. Noh, S. Hong, and B. Han, “Learning deconvolution network for semantic segmentation,” in *Proceedings of the IEEE international conference on computer vision*, 2015, pp. 1520–1528.
- [28] G. Huang, Z. Liu, L. Van Der Maaten, and K. Q. Weinberger, “Densely connected convolutional networks,” in *Proceedings of the IEEE conference on computer vision and pattern recognition*, 2017, pp. 4700–4708.
- [29] D. P. Kingma and J. Ba, “Adam: A method for stochastic optimization,” *CoRR*, vol. abs/1412.6980, 2014.
- [30] F. Milletari, N. Navab, and S.-A. Ahmadi, “V-net: Fully convolutional neural networks for volumetric medical image segmentation,” in *2016 Fourth International Conference on 3D Vision (3DV)*. IEEE, 2016, pp. 565–571.
- [31] S. Santurkar, D. Tsipras, A. Ilyas, and A. Madry, “How does batch normalization help optimization?” in *Advances in Neural Information Processing Systems*, 2018, pp. 2483–2493.
- [32] H. Li, Z. Xu, G. Taylor, C. Studer, and T. Goldstein, “Visualizing the loss landscape of neural nets,” in *Advances in Neural Information Processing Systems*, 2018, pp. 6389–6399.
- [33] A. Paszke, S. Gross, F. Massa, A. Lerer, J. Bradbury, G. Chanan *et al.*, “Pytorch: An imperative style, high-performance deep learning library,” in *Advances in Neural Information Processing Systems*, 2019, pp. 8024–8035.
- [34] J. Koizumi, Y. Yoshida, T. Nakazawa, and G. Ooneda, “Experimental studies of ischemic brain edema. 1. a new experimental model of cerebral embolism in rats in which recirculation can be introduced in the ischemic area,” *Jpn J stroke*, vol. 8, pp. 1–8, 1986.
- [35] A. Fenster and B. Chiu, “Evaluation of segmentation algorithms for medical imaging,” *2005 IEEE Engineering in Medicine and Biology 27th Annual Conference*, pp. 7186–7189, 2005.
- [36] E. Bribiesca, “An easy measure of compactness for 2d and 3d shapes,” *Pattern Recognition*, vol. 41, no. 2, pp. 543–554, 2008.
- [37] G. Rote, “Computing the minimum hausdorff distance between two point sets on a line under translation,” *Information Processing Letters*, vol. 38, no. 3, pp. 123–127, 1991.
- [38] Ö. Çiçek, A. Abdulkadir, S. S. Lienkamp, T. Brox, and O. Ronneberger, “3d u-net: learning dense volumetric segmentation from sparse anno-

tation,” in *International conference on medical image computing and computer-assisted intervention*. Springer, 2016, pp. 424–432.